Supplementary figures and material and methods

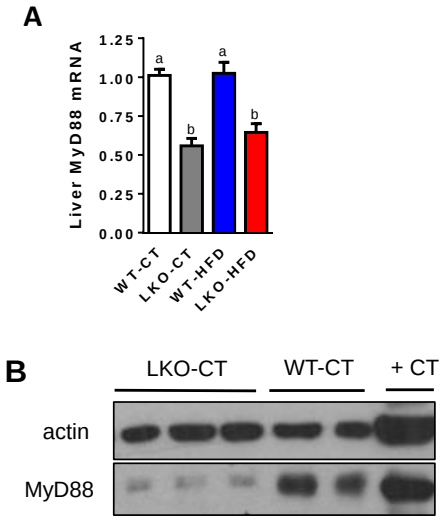

Figure S1: Validation of hepatocyte MyD88 deletion

(**A**) mRNA expression of *Myd88* in the liver of LKO mice and WT under CT diet and HFD (n=31-40). Data are presented as the mean ± SEM. Data with different superscript letters are significantly different ($p < 0.05$) according to post-hoc ANOVA one-way statistical analysis. (**B**) Representative liver immunoblot of MyD88 and β-actin in WT mice and LKO mice. + CT, corresponds to positive control protein (uterus).

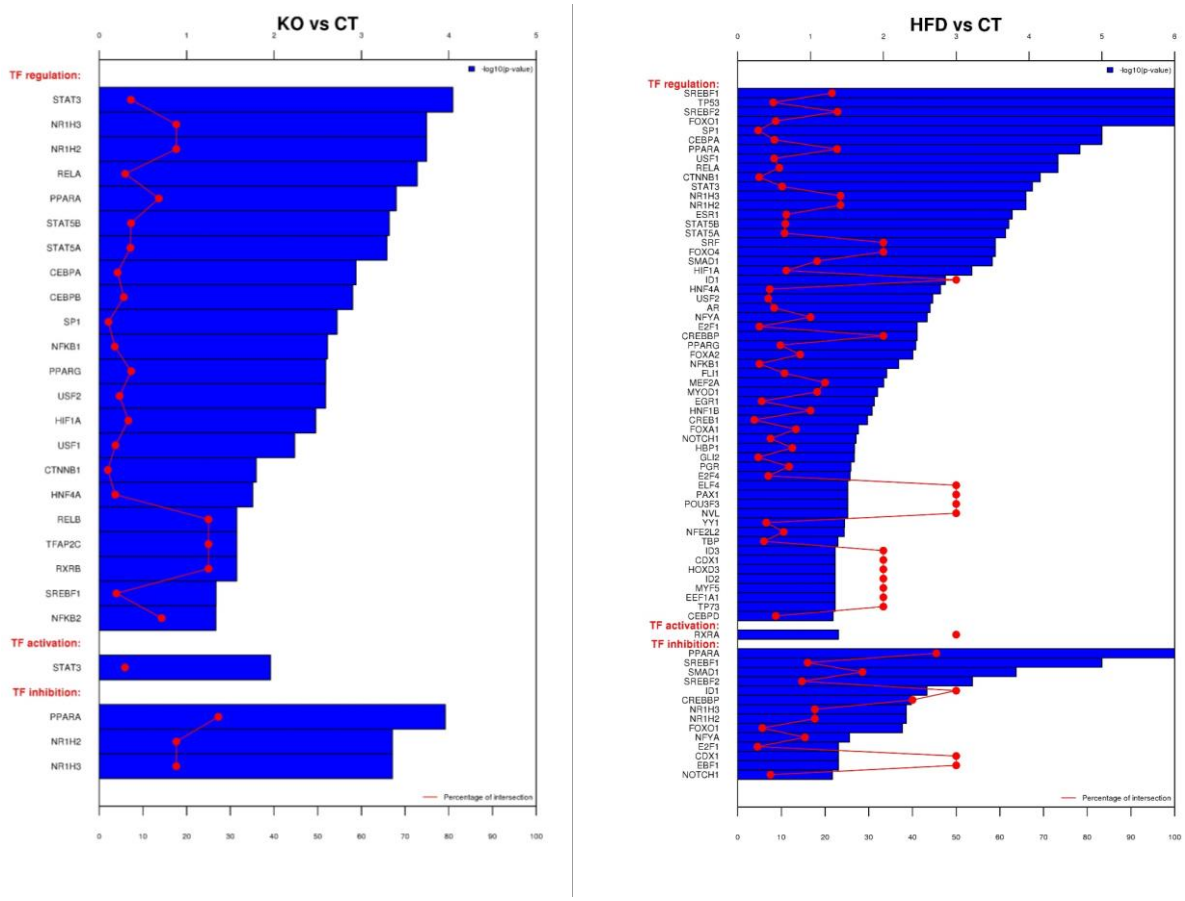

Figure S2: TFactS analysis of h**epatocyte *Myd88* deletion and HFD treated mice**

Transcription factor predictions by TFactS. The list of genes that were significantly modified in LKO-CT mice compared to WT-CT mice and WT-HFD compared to WT-CT was submitted to TFactS. The number of genes in the intersection between the submitted lists and the interrogated databases is presented as a percentage. The regulation type of transcription factors (activation or inhibition) is indicated if it was found significant ($p < 0.05$) by TFactS (sign-sensitive). Only transcription factors with a minimum of five target genes in the catalogue were considered.

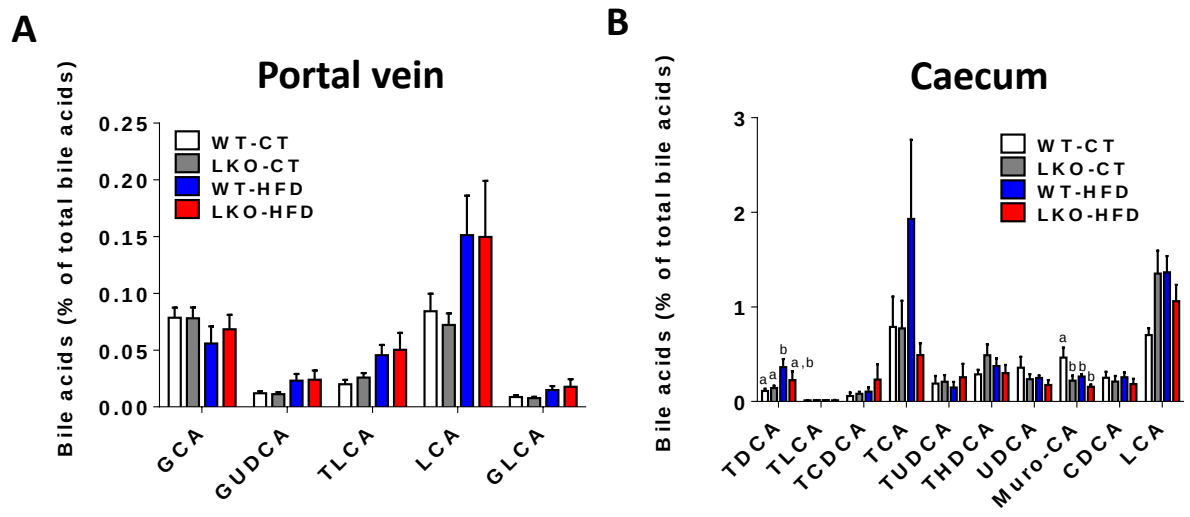

Figure S3: Hepatocyte *Myd88* deletion affects plasma bile acids profile

(**A**) Plasma bile acids (% of total bile acids), (**B**) Caecum bile acids. CA: cholic acid; UDCA: ursodeoxycholic acid; LCA: lithocholic acid; DCA: deoxycholic acid; CDCA: chenodeoxycholic acid; HDCA: hyodeoxycholic acid; Muro-CA: muricholic acid (T: taurine conjugated species; G: glycine conjugated species). Data are presented as the mean ± SEM (n=9-10). Data with different superscript letters or symbols are significantly different ($p < 0.05$) according to post-hoc one-way ANOVA.

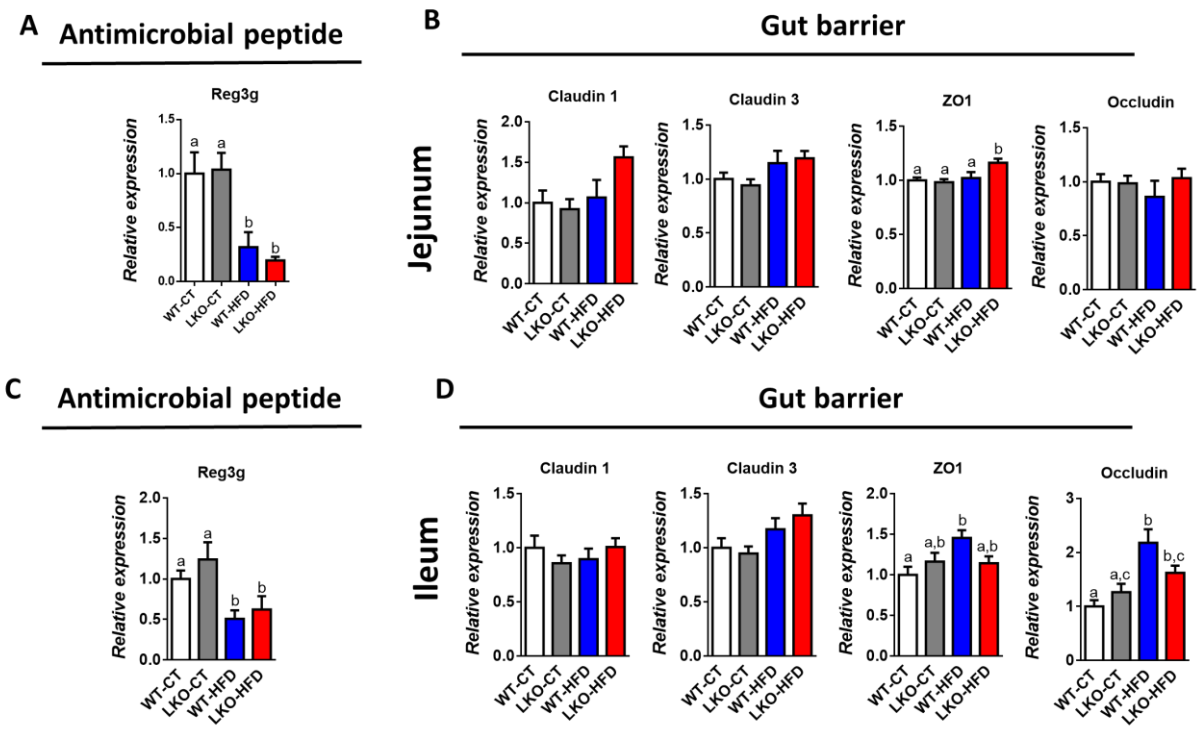

Figure S4: Markers of gut barrier function in the jejunum and in the ileum.

Antimicrobial peptide : Reg3g mRNA in the jejunum (**A**) and in the ileum (**C**). Markers of tight junction proteins (Claudin 1 and 3, ZO1 and occludin) in the jejunum (**B**) and in the ileum (**D**) of WT-CT, LKO-CT, WT-HFD and LKO-HFD mice. Data are presented as the mean ± SEM (n=10-12). Data with different superscript letters are significantly different ($p < 0.05$) according to post-hoc one-way ANOVA.

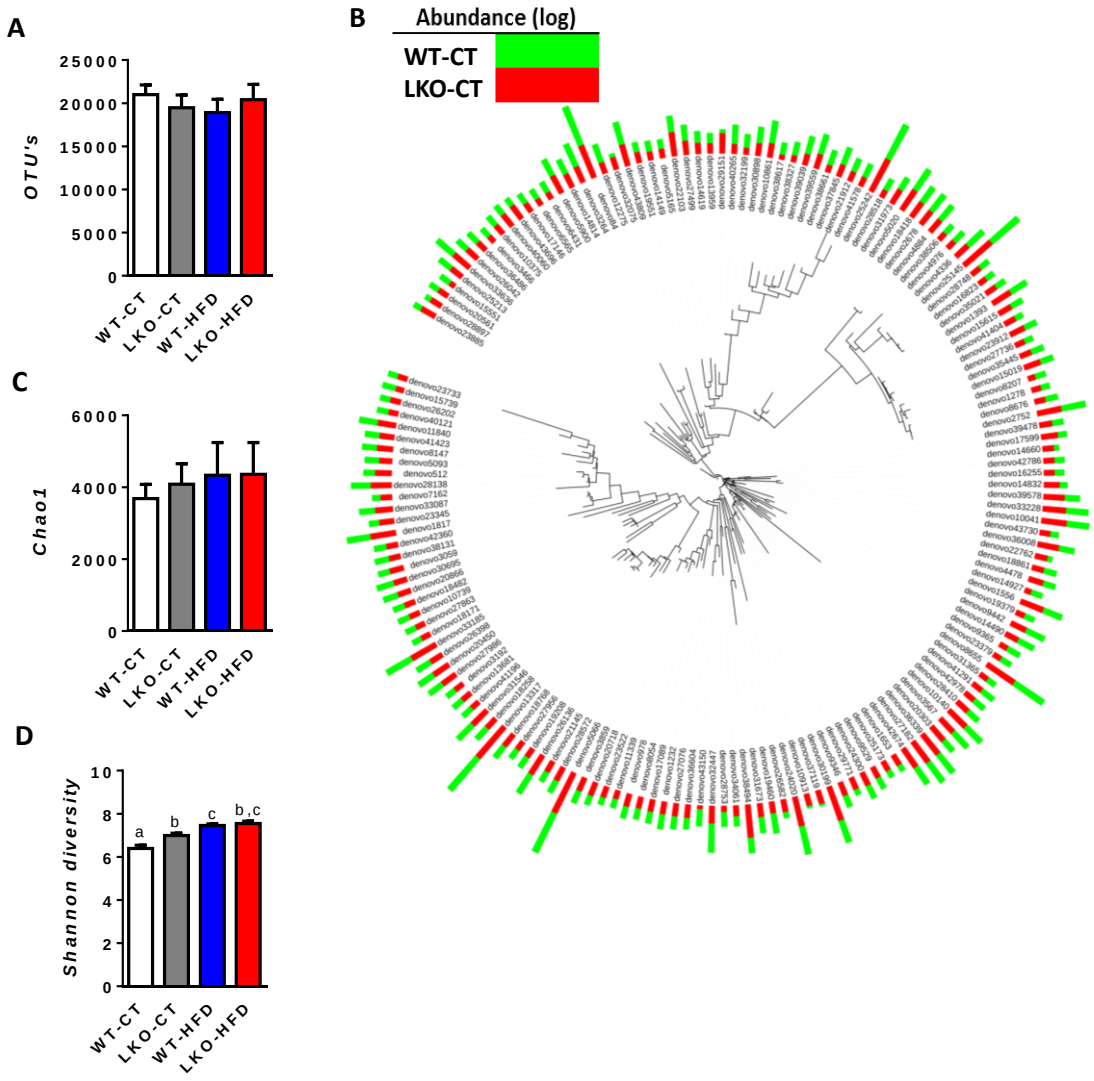

Figure S5: Gut microbiota markers of diversity and richness

(**A**) Mean number of operational taxonomic units (OTU's), (**B**) The tree was built with fasttree using representative sequences of OTUs as input. Only OTUs which contained more than 10 sequences (median number in all the samples from the STD group) were used. Abundance is represented as the log of the median number of sequences in the OTUs. The taxonomic identification of the 10 most abundant OTUs is given as indication. In brackets: highest level of taxonomic identification: p = phylum; f = family; g = genus. (**C**) Chao1 richness (**D**) Shannon diversity. Data are presented as the mean ± SEM (n=12). Data with different superscript letters are significantly different ($p < 0.05$) according to post-hoc one-way ANOVA.

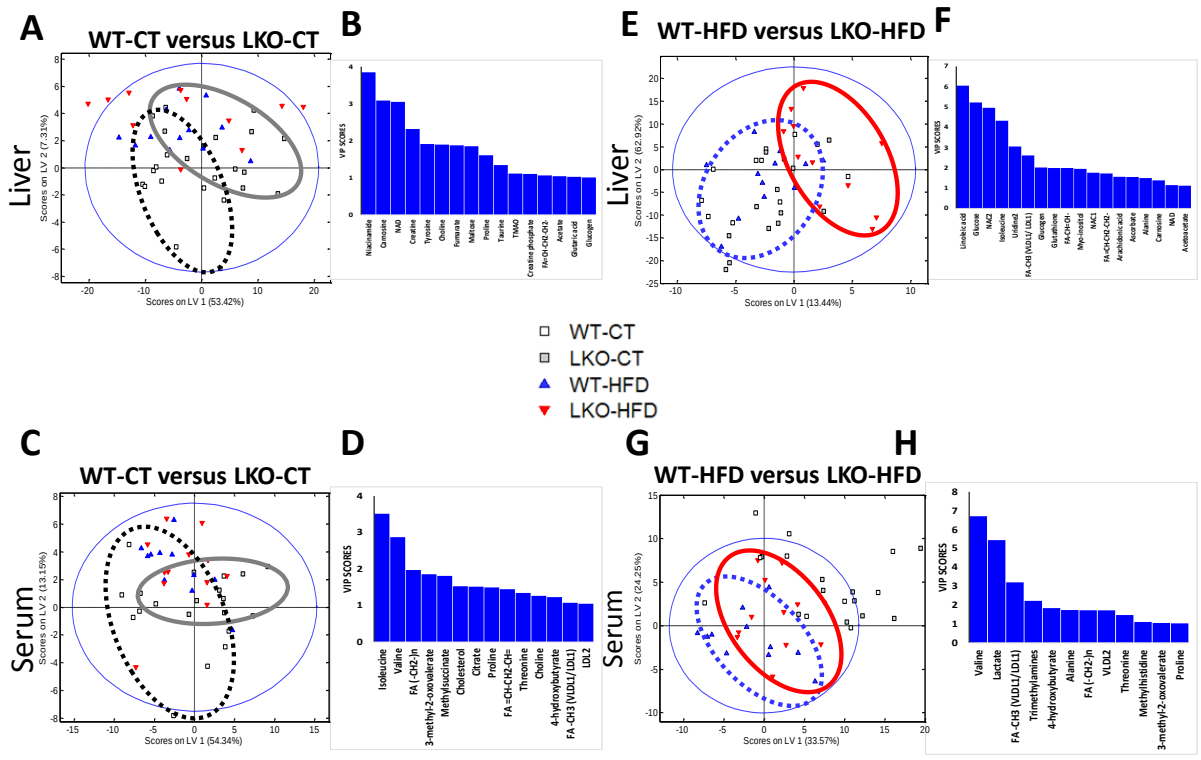

Figure S6. PLS DA analysis of the effect of deletion of MyD88 on the metabolome.

(**A-D**) PLS-DA scores plot and VIP scores for discrimination models based on liver metabolome (R2CV 0.115, RMSECV 0.743) (**A, B**) and serum metabolome (R2CV 0.104, RMSECV 0.723) **(C, D)** for discrimination between WT and LKO under CT treatment. Only samples from animals under CT treatment have been used to build the model. Samples from animals under HFD treatment (both WT and LKO) have been projected into the scores plot to seek for further metabolomic similarities.

(**E-F**) PLS-DA scores plot based and VIP scores for discrimination models based on liver metabolome (R2CV 0.198, RMSECV 0.755) **(E, F**) and the serum metabolome (R2CV 0.003, RMSECV 0.765) **(G, H)** for discrimination between WT and LKO under HFD treatment. Only samples from animals under HFD treatment have been used to build the model. Samples from animals under CT treatment (both WT and LKO) have been projected into the scores plot to seek for further metabolomic similarities.

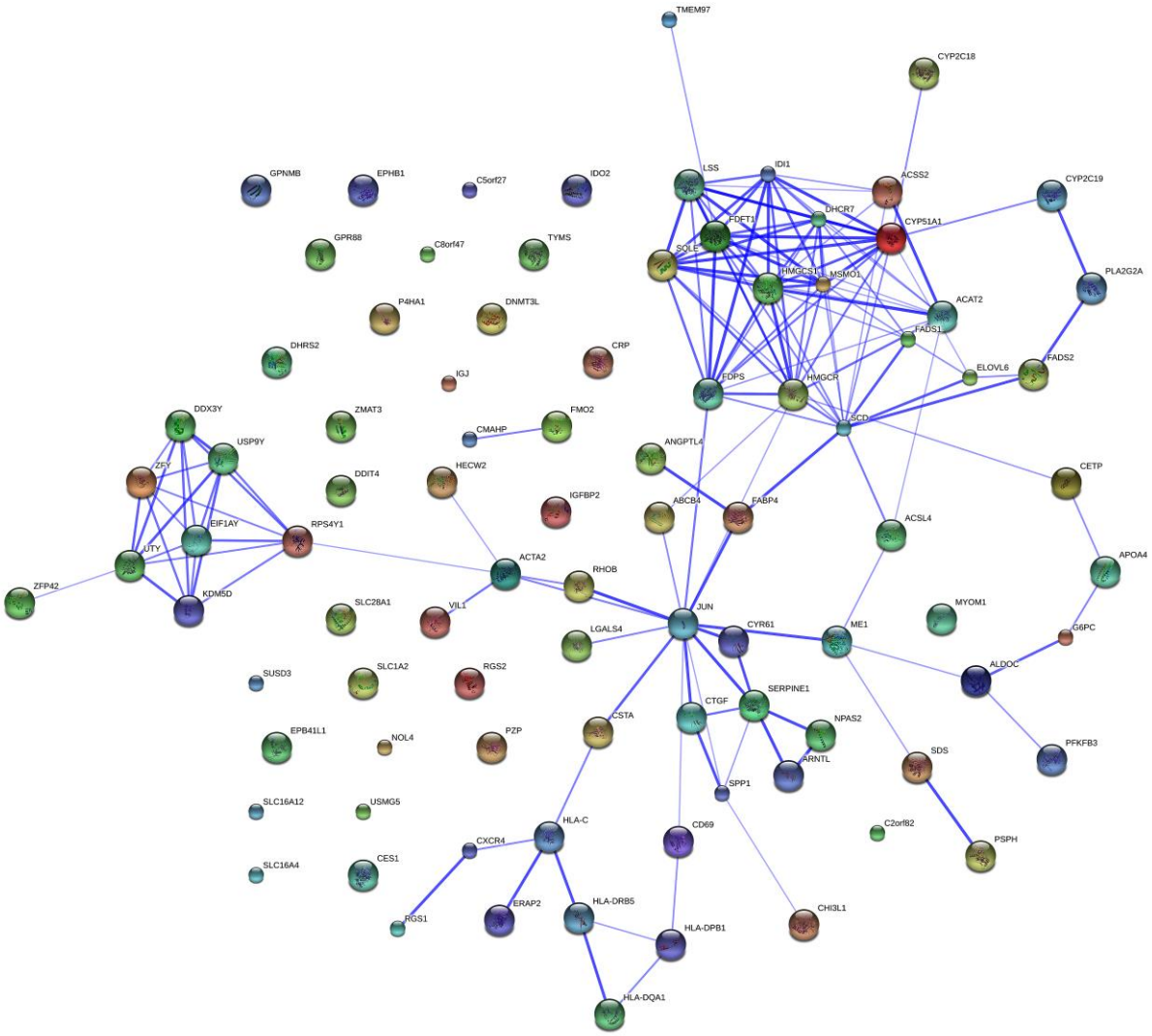

Figure S7 Graphic representation of the reported interactions between the differentially expressed genes between OBESE and NASH patients. All genes with a fold change greater than 2log +1 or below 2log -1 were loaded into the STRING 10 software. Predicted interactions are indicated with a blue line.

Documents with DAVID files are tables of biological processes affected in LKO-CT mice, WT-HFD mice and LKO-HFD mice compared to WT-CT mice. Biological processes similarly affected in LKO-CT mice and LKO-HFD mice, in LKO-CT mice and WT-HFD mice, in WT-HFD mice and LKO-HFD mice and biological processes similarly affected in LKO-CT, WT-HFD and LKO-HFD are also represented. These tables have been generated using the David web tool.

Supplementary online Material and Methods.

Mice were anaesthetized with isoflurane (Forene®, Abbott, Queenborough, Kent, England) after a 5 h-fast. Portal and cava vein blood samples were harvested for further analysis. After exsanguination, the mice were killed by cervical dislocation, and tissues were sampled. Adipose tissue deposits (mesenteric, epididymal, and subcutaneous), the liver, intestinal segments and the *tibialis anterior* (TA) skeletal muscles were precisely dissected, weighed, immediately immersed in liquid nitrogen and stored at -80°C until further analysis.

Indirect calorimetry studies in metabolic chambers

A set of 10 weeks-old WT and LKO mice were fed a control diet (CT) (10% fat, AIN93Mi, Research Diet, New Brunswick, NJ, USA) (WT-CT or LKO-CT) or a high-fat diet (HFD) (60% fat, D12492i Research Diet, New Brunswick, NJ, USA) (WT-HFD or LKO-HFD) (20 mice, n=4-6/group) for 8 weeks. The mice were then placed for one week in metabolic chambers (Labmaster, TSE Systems GmbH, Bad Homburg, Germany). Mice were housed individually, with free access to food and water. VO_2, VCO_2, physical activity and total energy expenditure were precisely recorded for 5 consecutive days.

Microarray analysis

Equal amounts of RNA from at least 10 mice per group were pooled within each group. Microarrays were performed as previously described [1]. The expression profile of several genes (up to 25) has been confirmed by using qPCR from individual animals, not from a pool of RNA. Mouse gene ST microarray chips were used for hybridization (MoGene 2.0 ST, Affymetrix®) the total number of genes covered by the probes is about 35240 genes, 28960 passed the signal filter. A GeneChip WT PLUS Reagent Kit (Affymetrix ®) was used for cRNA preparation from total RNA. Hybridization, washing and scanning were performed

according to the Affymetrix kits and procedures specific to the mouse gene ST chips. After the scanning was complete, the hybridization quality controls were checked using Affymetrix Gene Expression Console software. Using the Affymetrix APT suite tools, we normalized the data by the RMA-Sketch procedure and computed the signal detection p-values using the DABG algorithm. All the probe sets that had a DABG p-value above 0.05 in all conditions were discarded from the analysis. The rest of the probe sets were kept for fold-change analysis. Functional annotation and pathway analysis were performed using the DAVID web tool [2]. The prediction of the transcription factors regulated (inhibited or activated) by the different conditions was made using the TFactS web tool [3]. Analyses using both web tools were performed with a list of selected official gene names (the selection of genes was made using the threshold of 1.5-fold change versus WT-CT or versus WT-HFD) as input, and the threshold of significance was set by default to p-values below 0.05. All the graphs (Venn diagram, heat map and bar plot) related to the microarray analysis were generated using R scripts.

DNA isolation from mouse caecal samples for sequencing

Caecal contents were collected and kept frozen at -80°C until use. Metagenomic DNA was extracted from the caecal content using a QIAamp DNA Stool Mini Kit (Qiagen, Hilden, Germany) according to the manufacturer's instructions with modifications [4].

Bacterial DNA sequencing

The 16S rRNA gene was amplified from the caecal microbiota of the mice using the following universal eubacterial primers: 27Fmod (5'-AGRGTTTGATCMTGGCTCAG-3') and 519Rmodbio (5'-GTNTTACNGCGGCKGCTG-3'). Purified amplicons were sequenced utilizing Roche 454 FLX titanium instruments and reagents following the manufacturer's guidelines. Sequencing was performed at MR DNA (www.mrdnalab.com, Shallowater, TX,

USA). The number of raw sequences from the sequencing output was 1070821. Sequences were demultiplexed and processed using the QIIME pipeline (v1.7 using default options (Q25, minimum sequence lenght = 200 bp, maximum sequence length = 1000 bp, maximum number of ambiguous bases = 6, maximum number of homopolymers = 6, maximum number of primer mismatchs = 0). After quality processing, 957250 sequences (83.4%) remained. For the 48 samples analyzed, 43881 OTUs have been identified (97% similarity). The minimum number of sequences per sample was 9741 and the maximum number of sequences per sample was 29605. The median number of sequences per sample was 20886 and the mean number of sequences per sample was 19942.71 +/- 5027.019 (standard deviation). The Q25 sequence data derived from the sequencing process were analyzed with the QIIME 1.7 pipeline.

Briefly, sequences were depleted of barcodes and primers. Sequences <200 bp or >1000 bp were then removed; sequences with ambiguous base calls and with homopolymer runs exceeding 6 bp were also removed. Sequences were denoised, and operational taxonomic units (OTUs) were generated. Chimeras were also removed. OTUs were defined by clustering at 3% divergence (97% similarity). Final OTUs were taxonomically classified using BLASTn against a curated Greengenes database. PCoA was generated with QIIME using the unweighted UniFrac distance matrix between the samples [5, 6] and as previously described [7, 8].

Oral glucose tolerance test (OGTT)

After the mice underwent 7 weeks of treatment, an OGTT was performed as previously described [7].

Insulin tolerance test (ITT)

After the mice underwent 7 weeks of treatment, 5 hour-fasted mice were intraperitoneally injected with insulin (0.75 mU/g). Blood was collected from the tail vein at time 0 and after 15, 30, 45, 60 min for determination of glucose levels.

Insulin resistance index

The insulin concentrations in plasma samples collected from tail blood during OGTT were measured using an ELISA kit (Mercodia, Uppsala, Sweden) according to the manufacturer's instructions. The insulin resistance index was calculated by multiplying the area under the curve of both the blood glucose (-30 to 120 min) and the plasma insulin (-30 to 15 min) obtained from the OGTT.

Insulin signaling

To analyze the insulin signaling pathway, mice received insulin 1mU/g (Actrapid; Novo Nordisk A/S, Denmark) under anesthesia (isoflurane, Forene®, Abbott, Queenborough, Kent, England), or an equal volume of PBS into the portal vein to analyze signaling response to insulin. Three min after injection, mice were euthanized and liver were rapidly dissected.

Plasma ALT/AST

Plasma alanine-aminostransferase (ALT) and aspartate-aminotransferase (AST) activities were measured using kits coupling the enzymatic activity of interest with a $NADH+H^+$-dependent enzymatic reaction and spectrophotometric detection of $NADH+H^+$ conversion to NAD^+ (Diasys Diagnostic Systems, Holzheim, Germany) according to the manufacturer's instructions.

Liver lipid content

Total lipids were measured in the liver tissue after extraction in $CHCl_3$:MeOH according to Folch et al. [9] and adapted as previously described [10]. Briefly, 100 mg of liver tissue was homogenized in 1 ml of phosphate buffer (pH 7.4) using Ultra-Turrax (IKA, T10 basic, Boutersem, Belgium) until complete tissue lysis. Lipids were extracted by mixing 125 µl of lysates with 1 ml of $CHCl_3$:MeOH (2:1). The chloroform phase was evaporated under nitrogen flux, and the dried residue was solubilized in 100 µl of isopropanol. Triglycerides were measured using kits coupling enzymatic reaction and spectrophotometric detection of reaction end products (Diasys Diagnostic and Systems, Holzheim, Germany). Protein concentrations were measured by the Bradford method using bovine serum albumin as a standard.

Histological analysis

Slides preparation

A fraction of the main liver lobe was mounted in OCT embedding medium (Tissue-tek, Sakura, The Netherlands), sliced in 5µm thick sections and stored at -80°C until further analysis. Before histological staining, the frozen tissue sections were fixed in ice-cold 4% formaldehyde solution diluted in methanol for 5min.

Stainings

Liver steatosis was visualized by Oil Red O staining. The sections were stained with 0.5% Oil red O solution in propylene glycol for 10 min at 60°C. The slides were transferred to an 85% propylene glycol solution for 1 min, rinsed in distilled water for 2 changes, and processed for hematoxylin counter staining. The sections were then cleared in Xylene, mounted with DPX and coverslipped.

Liver fibrosis was visualized by Picrosirius red. The samples were incubated for 90 min in 0.1% Sirius red F3B (Sigma) dissolved in saturated picric acid. After rinsing twice in acidified water and in distilled water, sections were briefly dehydrated with increasing concentrations of ethanol. The sections were then cleared in Xylene, mounted with DPX and coverslipped.

General morphology of the liver was assessed on Hematoxylin and Eosin (H&E) stained sections using a standard protocol.

To visualize inflammatory cells a F4/80 staining was performed. After fixation, endogenous peroxidase activity was quenched with 0.3 % H_2O_2 in methanol for 20 minutes. Following blocking in TSA TNB (Perkin Elmer, Waltham, MA, USA) for 1 hour, sections were incubated overnight with specific rat anti-mouse primary antibodies directed against F4/80 (1:100; ab6640, Abcam, Cambridge, England) at room temperature. The following day, slides were incubated with a rabbit anti-rat secondary antibody for 2h (1:200; 312-065-003, Jackson ImmunoResearch Laboratories, West Grove, PA, USA), followed by incubation for 30 minutes with an anti-rabbit HRP-Labeled Polymer (Envision kit, Dako). Peroxidase activity was revealed using diaminobenzidine (Dako). Slides were then briefly counterstained with Mayer's Hemalum solution (Merck, Darmstadt, Germany), dehydrated through a series of ethanol to xylene and mounted with DPX.

Image acquisition and analysis

Whole-mount sections were digitized using a whole-slide scanner (Leica SCN400, Leica Microsystems, Germany) and high-magnification images (20x or 40x) were captured using the Leica Image Viewer Software (Version 4.0.4). At least five pictures were taken per mouse, with 7 to 12 mice per group.

Quantification of fibrosis (% of Red stained area over total area) was performed automatically using ImageJ software (National Institutes of Health, version 1.48r).

The severity of the steatosis was scored on H&E stained liver sections based on the size and number of hepatic lipid droplets as proposed by Le Roy et al (Gut, 2013, PMID: 23197411). Scores were given as follow: 1) cells have no or a low amount of small lipid droplets (microvesicular pattern); 2) high amount of cells with a microvesicular pattern; 3) high number of cells with microvesicular pattern, mixed with cells containing large lipid droplest (macrovesicular pattern); 4) high amount of macrovesicular cells.

For inflammation, the scoring was based on the amount and density of F4/80 positive immune cells. Scores were as follow: 1) for dispersed cells in low numbers; 2) for dispersed cells in high numbers; 3) for dispersed cells in high numbers and presence of zones with dense foci; 4) for dispersed cells in higher numbers and presence of numerous infiltration foci.

Liver glycogen determination

Briefly, 30mg of powdered tissue stored at – 80°C were incubed with 200 ul of NaOH 1 M at 55°C for 1 h. Samples were mixed, neutralized with 200 ul HCl 1N, and then centrifuged at 7.0 g for 5 min at 4°C. Supernatant were removed, and 10 ul were incubated in 40 ul of a solution of amyloglucosidase 50 U/ml (Sigma) dilute in sodium acetate buffer 0.2 M (pH 7.4), while 10 ul were incubated in 40 ul of sodium acetate buffer only. The tubes were shaken for 1 h at 55°C. Then, 6 ul of each sample were deposited in 96-well plates with 200 ul of a biochemical reagent, incubated at 37°C for 10 min (Glucose God FS; Diasys). The DO was read at 505nm by spectrophotometry. The difference between conditions with amyloglucosidase and conditions with buffer only represented the glycogen content of the liver sample. Glycogen was expressed as milligrams of glucose resulting from glycogen hydrolysis per gram of tissue.

RNA extraction and real-time qPCR analysis

Total RNA was prepared from tissues using TriPure reagent (Roche). The quantification and integrity analysis of the total RNA were performed by running 1 μl of each sample on an Agilent 2100 Bioanalyzer (Agilent RNA 6000 Nano Kit, Agilent). The cDNA was prepared by reverse transcription, and real-time qPCR was performed as previously described [11]. *RPL19* was chosen as the housekeeping gene. The primers are shown in Table S6.

SDS-PAGE and immunoblotting for MyD88

To obtain total lysates, liver were homogenized with TissueLyser II (Qiagen) in RIPA buffer, and the proteins were extracted as previously described [12]. Equal amounts of proteins (20 μg) were separated by SDS-PAGE and transferred to nitrocellulose membranes. The membranes were incubated overnight at 4 °C with antibody directed against MyD88 (1:500, sc-11356, Santa Cruz Biotechnology, Inc, USA) diluted in Tris-buffered saline-Tween 20 containing 1% non-fat dry milk. The loading control was β-actin.

Bile acid analysis

The extraction and analysis of bile acids were performed according to a previous work [13]. Briefly, bile acids were extracted by protein precipitation with 10 volumes of IS-containing methanol. After the samples were vortexed and centrifuged, the supernatant was diluted 50 times in methanol:water (1:1). Bile acid separation was performed using water and acetonitrile on a Kinetex C18 column (2.1 ×100 mm with 1.7 μm particles; Phenomenex, Torrance, CA, USA). Detection was performed using a QTRAP 5500 instrument (AB Sciex, Toronto, Canada) with MRM in negative mode.

NMR spectroscopy

The total preparation time for each sample before NMR detection was less than 5 min. Mouse serum samples were stored at -80°C and thawed before use. For NMR analysis, 20 μL of serum was mixed with 2 μL of D_2O (as a field lock). In total, 20 μL of the mixture of each sample was then transferred into a 1 mm high-quality NMR capillary.

Tissue samples were prepared without thawing to minimize metabolic degradation. All the materials to be in contact with the tissue were pre-cooled to reduce tissue degradation during the sample preparation process. Frozen samples were taken from the ultra-freezer and immediately placed in a cryo-vial in liquid N_2 until insertion into a 4-mm outer diameter ZrO_2 rotor. The HR-MAS tissue sample was taken from the whole frozen specimen submerged in liquid nitrogen. The pre-cooled rotor was filled with cooled D_2O after tissue sample insertion. Cylindrical inserts were used in all cases, limiting the inner rotor volume to 50 μl. Excess D_2O was removed before rotor sealing. Tissue samples were weighted in the rotor before D_2O addition and HR-MAS measurements. Tissue fragments were weighted exclusively for sample preparation purposes. The mean sample weight was 35 ± 9 mg.

All ^{1}H NMR spectra were acquired using a standard one-dimensional pulse sequence with water suppression (Bruker Avance 600 spectrometer operating at 600.13 MHz with a 1 mm $^{1}H/^{13}C/^{15}N$ TXI probe). In total, 256 FIDs (free induction decays) were collected into 64 k data points with a spectral width of 14 ppm and a recycle delay (RD) of 1 s. The water signal was saturated with weak irradiation during the recycle delay. Before Fourier transformation, the free induction decay was multiplied by a 0.3 Hz exponential line-broadening function. Spectral chemical shift referencing the Alanine CH_3 doublet signal at 1.475 ppm was performed in all spectra. We normalized the peak intensity to the total aliphatic spectral area. Spectral regions between 0.5 and 4.5 ppm and between 5.5 and 9.5 ppm were investigated. We used available spectral databases and 2D NMR experiments to aid in the structural identification of relevant metabolites. All spectra were processed using

MestReNova (MestreLab, Santiago de Compostela, Spain) and transferred to MATLAB® (MathWorks Inc, 2006) using in-house scripts for data analysis. Signals belonging to selected metabolites were integrated by restricted spectral binning and quantified using semi-automated in-house MATLAB peak-fitting routines. These fitting routines were based on Levenburg-Marquardt optimization procedures. The target function for the optimization included experimental spectra measured for standard solutions of selected metabolites with complex multiplet patterns and theoretically generated Lorentzian-shape signals for those metabolites with simpler spectral patterns.

We used PLS_Toolbox 5.0 (Eigenvector Research, WA, USA) for MATLAB® to build the principal component analysis (PCA) and the projection latent structures discriminant analysis (PLS-DA) models. The primary advantage of PCA and PLS-DA models is that the leading sources of variability in the data are modeled by new variables that explain most of the variance in the data and, consequently, in their associated scores and loadings, allowing the visualization and understanding of different patterns and relations in the data.

PCA is able to find low dimensional embedding of multivariate data in a manner that optimally preserves the structure of the data. PCA transforms variables in a data set into a smaller number of new latent variables called principal components (PCs), which are uncorrelated to each other and which account for decreasing proportions of the total variance of the original variables. Each new PC is a linear combination of the original variation such that a compact description of the variation within the data set is generated. Observations are assigned scores according to the variation measured by the principal component with those having similar scores being clustered together.

PLS-DA is a classification technique that encompasses the properties of partial least squares regression with the power of discriminant analysis [14]. From a mathematical point of view, PLS-DA is a supervised extension of PCA used to distinguish two or more classes by

searching for variables (X matrix) that are correlated to class membership (Y matrix). In this approach, the axes are calculated to maximize class separation and can be used to examine separation that would otherwise be across three or more principal components.

The PLS-DA models were cross-validated by the leave-one-out method. Cross validation is a very useful tool that provides two critical functions in chemometrics. First, cross validation enables an assessment of the optimal complexity of a model. Second, cross validation allows an estimation of the performance of a model when it is applied to unknown data. For a given data set, cross validation involves a series of experiments, hereby called sub-validation experiments, each of which involves the removal of a subset of individuals from a dataset, construction of a model using the remaining objects in the dataset, and subsequent application of the resulting model to the removed objects. Therefore, each sub-validation experiment involves testing a model with objects that were not used to build the model. Typical cross validation involves more than one sub-validation experiment by selecting different subsets of individuals for model building and testing. Leave-one-out cross validation involves the use of a single observation from the original sample as the validation data and the remaining observations as the training data. This process is repeated in a manner that each observation in the sample is used once as the validation data. The leave-one-out method is ideally suited for datasets with a limited number of samples.

Study population, liver histology and patient classification:

A cohort study included morbidly obese patients undergoing bariatric surgery as previously described [15]. In short: a liver biopsy was performed using a 16G trucut biopsy needle for histopathological assessment and from which RNA was extracted. Histological scoring was performed by expert liver pathologists blinded to all clinical information. Features of NASH were semi-quantitatively scored according to the NASH-Clinical Research Network Scoring

System criteria [16]. Patients with proven cirrhosis or cases with borderline features of NASH were excluded for further analysis. We subsequently classified the patients into 3 distinct groups according their liver histology: Group 1 (OBESE CONTROL): patients with < 5% steatosis, NAS score for all patients in this group is 0; Group 2 (NAFL): NAFLD without evidence of inflammation or NASH, NAS score < 4, Group 3 (NASH): NASH without significant fibrosis, NAS score ≥ 5 and fibrosis score 0-1. All patients gave written informed consent and the study protocol was approved by the research institution ethical committee (KUL).

RNA-extraction, cDNA synthesis and Quantitative RT-PCR:

Liver tissue was homogenized with Trizol (Invitrogen Life Technologies, USA) and RNA isolated by means of RNeasy Kit (Qiagen, Chatsworth, CA). RNA quality and quantity was determined by NanoDrop spectrophotometer (NanoDrop Technologies, Centreville, DE) and Agilent 2100 BioAnalyzer (Agilent, Palo Alto, CA) respectively.

Microarray and Data Processing

A total of 100 ng per sample of total RNA spiked with bacterial RNA transcript-positive controls (Affymetrix) was amplified and labeled using the GeneChip 3' IVT express kit (Affymetrix). All steps were performed according to the manufacturer's protocol (Affymetrix). To assess the raw probe signal intensities, chips were scanned using a GeneChip scanner 3000 (Affymetrix). Analysis of the microarray data was performed in the R programming environment, in conjunction with the packages developed within the Bioconductor project [17]. The analysis was based on the RMA expression levels of the probe sets, computed with the package xps (version 1.16.0). Differential expression was assessed via the moderated t-statistic, described by Smyth et al, [18, 19] and implemented in the limma package (version 3.12.1). To control the false-discovery rate, multiple testing corrections were performed using the Benjamini-Hochberg's method [20].

Data are available through National Center for Biotechnology Information (GSE59045).

Supplemental References

1 Essaghir A, Dif N, Marbehant CY, Coffer PJ, Demoulin JB. The transcription of FOXO genes is stimulated by FOXO3 and repressed by growth factors. The Journal of biological chemistry 2009;284:10334-42.

2 Huang da W, Sherman BT, Lempicki RA. Systematic and integrative analysis of large gene lists using DAVID bioinformatics resources. Nature protocols 2009;4:44-57.

3 Essaghir A, Toffalini F, Knoops L, Kallin A, van Helden J, Demoulin JB. Transcription factor regulation can be accurately predicted from the presence of target gene signatures in microarray gene expression data. Nucleic acids research 2010;38:e120.

4 Everard A, Matamoros S, Geurts L, Delzenne NM, Cani PD. Saccharomyces boulardii Administration Changes Gut Microbiota and Reduces Hepatic Steatosis, Low-Grade Inflammation, and Fat Mass in Obese and Type 2 Diabetic db/db Mice. mBio 2014;5.

5 DeSantis TZ, Hugenholtz P, Larsen N, Rojas M, Brodie EL, Keller K, *et al.* Greengenes, a chimera-checked 16S rRNA gene database and workbench compatible with ARB. Appl Environ Microbiol 2006;72:5069-72.

6 McDonald D, Price MN, Goodrich J, Nawrocki EP, DeSantis TZ, Probst A, *et al.* An improved Greengenes taxonomy with explicit ranks for ecological and evolutionary analyses of bacteria and archaea. The ISME journal 2012;6:610-8.

7 Everard A, Geurts L, Caesar R, Van Hul M, Matamoros S, Duparc T, *et al.* Intestinal epithelial MyD88 is a sensor switching host metabolism towards obesity according to nutritional status. Nature communications 2014;5:5648.

8 Geurts L, Everard A, Van Hul M, Essaghir A, Duparc T, Matamoros S, *et al.* Adipose tissue NAPE-PLD controls fat mass development by altering the browning process and gut microbiota. Nature communications 2015;6:6495.

9 Folch J, Lees M, Sloane Stanley GH. A simple method for the isolation and purification of total lipides from animal tissues. JBiolChem 1957;226:497-509.

10 Geurts L, Everard A, le Ruyet P, Delzenne NM, Cani PD. Ripened dairy products differentially affect hepatic lipid content and adipose tissue oxidative stress markers in obese and type 2 diabetic mice. J Agric Food Chem 2012;60:2063-8.

11 Everard A, Lazarevic V, Gaia N, Johansson M, Stahlman M, Backhed F, *et al.* Microbiome of prebiotic-treated mice reveals novel targets involved in host response during obesity. The ISME journal 2014;8:2116-30.

12 Pachikian BD, Essaghir A, Demoulin JB, Neyrinck AM, Catry E, de Backer FC, *et al.* Hepatic n-3 polyunsaturated fatty acid depletion promotes steatosis and insulin resistance in mice: genomic analysis of cellular targets. PLoSONE 2011;6:e23365.

13 Tremaroli V, Karlsson F, Werling M, Stahlman M, Kovatcheva-Datchary P, Olbers T, *et al.* Roux-en-Y Gastric Bypass and Vertical Banded Gastroplasty Induce Long-Term Changes on the Human Gut Microbiome Contributing to Fat Mass Regulation. Cell Metab 2015;22:228-38.
14 Trygg J, Holmes E, Lundstedt T. Chemometrics in metabonomics. Journal of proteome research 2007;6:469-79.
15 du Plessis J, van Pelt J, Korf H, Mathieu C, van der Schueren B, Lannoo M, *et al.* Association of Adipose Tissue Inflammation With Histologic Severity of Nonalcoholic Fatty Liver Disease. Gastroenterology 2015;149:635-48 e14.
16 Brunt EM, Kleiner DE, Wilson LA, Belt P, Neuschwander-Tetri BA, Network NCR. Nonalcoholic fatty liver disease (NAFLD) activity score and the histopathologic diagnosis in NAFLD: distinct clinicopathologic meanings. Hepatology 2011;53:810-20.
17 Gentleman RC, Carey VJ, Bates DM, Bolstad B, Dettling M, Dudoit S, *et al.* Bioconductor: open software development for computational biology and bioinformatics. Genome Biol 2004;5:R80.
18 Smyth GK. Linear models and empirical bayes methods for assessing differential expression in microarray experiments. Stat Appl Genet Mol Biol 2004;3:Article3.
19 Smyth GK, Michaud J, Scott HS. Use of within-array replicate spots for assessing differential expression in microarray experiments. Bioinformatics 2005;21:2067-75.
20 Benjamini Y, Hochberg, Y. Controlling the false discovery rate: a practical and powerful approach to multiple testing. Journal of the Royal Statistical Society Series B (Methodological) 1995;57:289-300.